Practical Approach to Orbital Lesions by Anatomic Compartments

Guilherme Gotti Naves, MD • Heytor José de Oliveira Cabral, MD • Helen Ribeiro de Oliveira, MD • Thiago Luiz Pereira Donoso Scoppetta, MD
Henrique Bortot Zuppani, MD • Fernanda Boldrini Assunção, MD

Author affiliations, funding, and conflicts of interest are listed at the end of this article.

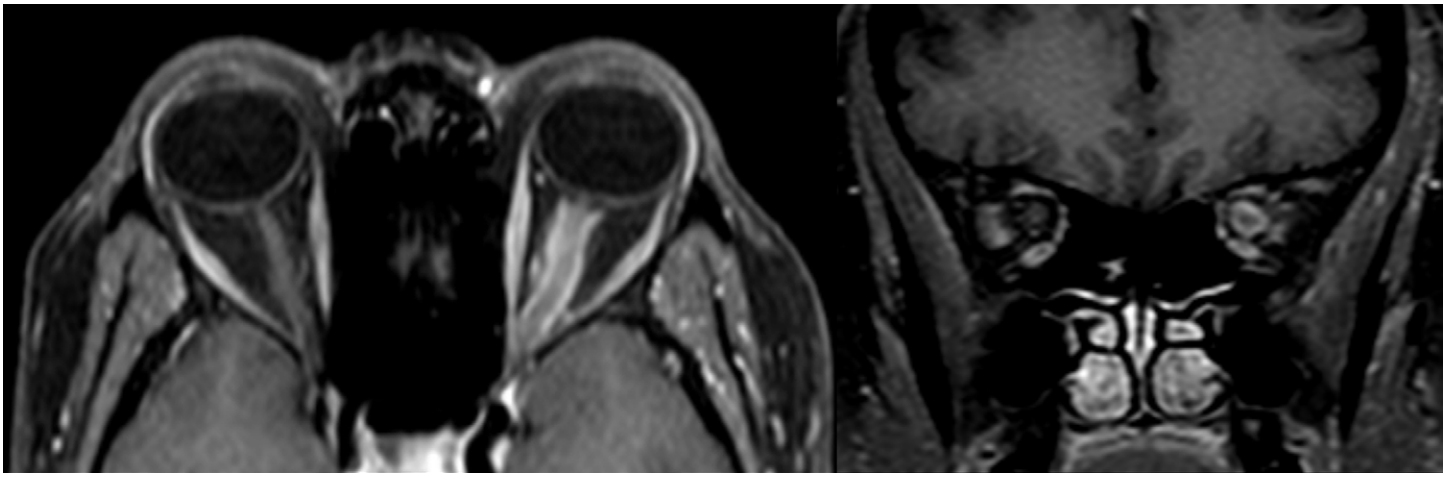

A wide range of pathologic conditions can originate in the orbit. While it is common to approach the differential diagnosis based on disease categories, such as neoplastic and inflammatory, segmenting the orbit into anatomic compartments can direct the radiologist toward the most common pathologic conditions for each manifestation and space. The orbit can be divided into intraconal, conal, and extraconal compartments. Additionally, the optic nerve sheath complex and lacrimal apparatus can be partitioned into separate compartments due to their unique functions and pathologic features. By using this anatomic approach, the authors review the most common pathologic conditions affecting the orbit and discuss clinical and imaging findings that can guide the differential diagnosis for lesions with similar appearances.

Introduction

A broad range of pathologic conditions can arise in the orbit, rendering clinical diagnosis particularly challenging given the frequent overlap in clinical features. Cross-sectional imaging is an important tool for characterizing orbital lesions, confirming clinical suspicions, and narrowing the differential diagnosis. While it is common to approach the differential diagnosis based on disease categories, such as neoplastic and inflammatory, dividing the orbit into anatomic compartments can direct the radiologist to consider the most common pathologic conditions for each presentation and space.

The orbit can be divided into intraconal, conal, and extraconal compartments. For diagnostic purposes, it is also beneficial to delineate the optic nerve sheath complex (ONSC) and globe within the intraconal compartment and the lacrimal apparatus within the extraconal compartment due to their distinctive functions and pathologic features (Figs 1, 2).

CT is often the first imaging modality performed due to its availability and fast acquisition. Nevertheless, MRI provides better soft-tissue contrast, making it the preferred modality for assessing the globe, ocular muscles, ONSC, and orbital fat. Signal intensity on T1-weighted and T2-weighted images is described in comparison with that of the normal extraocular muscles (EOMs). The ONSC is a noteworthy exception. As an extension of the central nervous system, it is best evaluated using the contralateral nerve for comparison. When both optic nerves are affected, the signal intensity is compared with that of brain white matter.

This article reviews the clinical and imaging features of the most common pathologic conditions affecting each orbital anatomic compartment. A summary is presented at the conclusion of the article, highlighting imaging features and clinical insights.

Optic Nerve Sheath Complex

The ONSC is formed by the optic nerve and its dural and leptomeningeal coverings, which extend from the intracranial meninges to the globe. Cerebrospinal fluid fills the space

Supplemental Material | TestYour Knowledge CME

RadioGraphics 2024;44(10):e240026
https://doi.org/10.1148/rg.240026

Content Codes: CT, MR, NR

Abbreviations: CVM = cavernous venous malformation, EOM = extraocular muscle, IgG4 = immunoglobulin G4, IH = infantile hemangioma, ION = ischemic optic neuropathy, LM = lymphatic malformation, NF1 = neurofibromatosis 1, ONSC = optic nerve sheath complex, TED = thyroid eye disease

TEACHING POINTS

- Restricted diffusion and the bright spot sign are the main imaging features that suggest ION.
- A progressive enhancement pattern is a characteristic finding of CVMs, exhibiting initial poor and heterogeneous central enhancement on CT and MR images, with subsequent filling and homogeneous intensity on delayed images.
- The involvement of EOMs in TED typically affects multiple muscles and follows a characteristic pattern: the *i*nferior rectus is most frequently affected, followed by *m*edial rectus, superior rectus, *l*ateral rectus, and *o*blique muscles ("I'M SLOw" mnemonic).
- Restricted diffusion is a characteristic finding distinguishing rhabdomyosarcoma from lesions with similar features, such as IHs.
- Neurofibromas can manifest with a hyperintense rim surrounding a central hypointense area on T2-weighted images ("target" sign), whereas schwannomas commonly manifest with central hyperintensity surrounded by hypointensity on T2-weighted images due to hemorrhagic or cystic degeneration.

between the optic nerve sheath and the optic nerve. Anatomically, the optic nerve can be divided into intraocular, intraorbital, intracanalicular, and intracranial segments.

Optic Neuritis

Optic neuritis is an inflammatory optic neuropathy characterized by acute or subacute vision loss with periocular pain and painful eye movements. The majority of cases are caused by demyelinating disease, which may be isolated or occur in the setting of a primary demyelinating condition such as multiple sclerosis. Patients with multiple sclerosis have progressive unilateral symptoms that occur over several days and improve over the course of 2–3 weeks (1,2).

Optic neuritis associated with multiple sclerosis is characteristically unilateral, involving the anterior intraorbital segment of the optic nerve (Fig 3). MRI findings include contrast enhancement, T2 hyperintensity, and occasional diffusion restriction of the nerve. Alternate diagnoses should be considered when optic neuritis involvement is bilateral, when more than 50% of the nerve is affected, or when there is posterior intraorbital optic neuritis or chiasm involvement (1,3).

Other demyelinating disorders associated with optic neuritis include neuromyelitis optica and myelin oligodendrocyte glycoprotein antibody–associated disease, as well as autoimmune and infectious diseases such as sarcoidosis and herpes zoster infection. These entities can be differentiated from multiple sclerosis based on clinicoradiologic features (1,2).

Neuromyelitis optica is an autoimmune demyelinating disease characterized by antibodies targeting the astrocyte

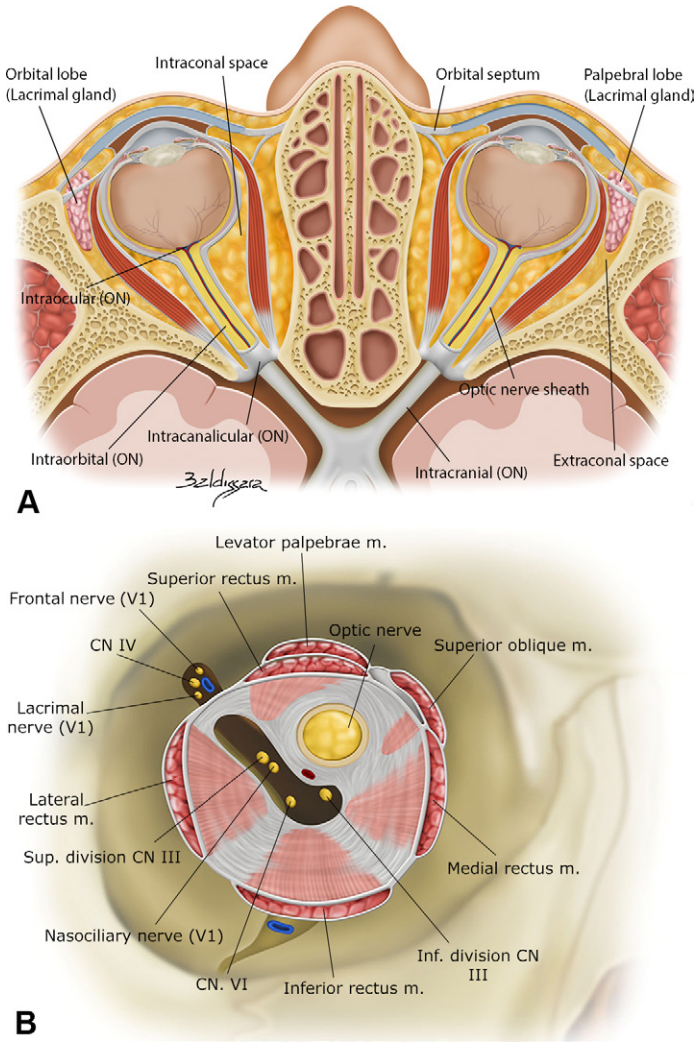

Figure 1. Relevant orbital anatomy. **(A)** Axial view shows normal orbital structures. The orbit is composed of four walls: medial, lateral, superior, and inferior. The medial wall is formed by the lamina papyracea, and the inferior wall corresponds to the roof of the maxillary sinus. *ON* = optic nerve. **(B)** Illustration of the conal compartment and orbital apex shows the annulus of Zinn and its relation to nerves in the muscle cone. *CN* = cranial nerve, *Inf.* = inferior, *m.* = muscle, *Sup.* = superior

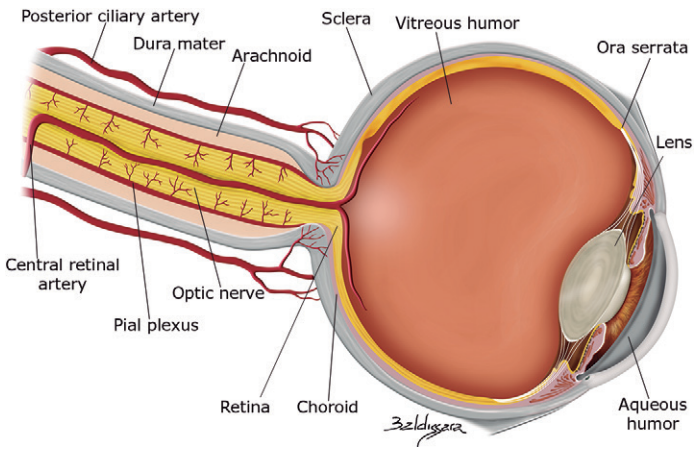

Figure 2. Illustration of the ONSC and globe shows the optic nerve and its dural and leptomeningeal coverings, as well as relevant globe anatomy.

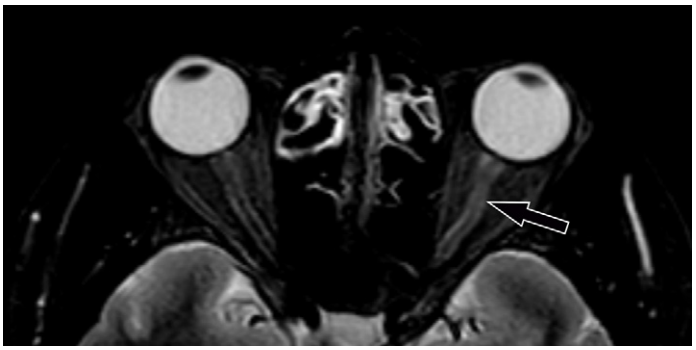

Figure 3. Optic neuritis associated with multiple sclerosis in a 40-year-old woman who presented with left vision loss. Axial fat-saturated T2-weighted MR image shows left optic nerve hyperintensity, relative to the contralateral nerve, involving the anterior intraorbital segment (arrow) and affecting less than 50% of the nerve.

aquaporin water channel. At MRI, optic neuritis typically manifests as bilateral longitudinally extensive lesions involving more than 50% of the nerve length and preferentially affecting the posterior optic pathway (Fig S1) (1,4).

Myelin oligodendrocyte glycoprotein antibody–associated disease is a more recently recognized form of optic neuritis characterized by antibodies targeting myelin, a marker of mature oligodendrocytes. Distinctive imaging features include optic nerve head edema, bilateral longitudinally extensive optic neuritis, and enhancement of the nerve sheath (Fig S2) (1,2,5).

Ischemic Optic Neuropathy

Ischemic optic neuropathy (ION) is an acute disease caused by vascular insufficiency, leading to nerve dysfunction and necrosis. The optic nerve's blood supply derives from arterial networks of the ophthalmic artery, a branch of the internal carotid artery. The optic nerve can be divided into anterior and posterior segments based on vascular supply. The anterior segment is mainly supplied by the posterior ciliary arteries, while the posterior segment is supplied by pial branches of the ophthalmic artery and intraneural branches of the central retinal artery.

Anterior ION involves the optic nerve head and optic disc. Anterior ION is classified as nonarteritic, associated with small-vessel disease, or arteritic, mostly caused by giant cell arteritis (6,7). Posterior ION involves the remaining portion of the optic nerve and is also classified as either nonarteritic or arteritic (8). Clinically, ION manifests with sudden painless vision loss. Fundoscopy can help distinguish between anterior ION, manifesting with disc edema, and posterior ION, manifesting with a normal disc. The presence of new-onset temporal headache, jaw claudication, and elevated C-reactive protein levels are findings indicative of arteritic anterior ION (3,8).

MRI features include T2 hyperintensity of the optic nerve, reduced contrast enhancement, and restricted diffusion. In cases of anterior ION, ischemic edema of the nerve head may result in increased enhancement, leading to the "bright spot" sign. Restricted diffusion and the bright spot sign are the main imaging features that suggest ION (Figs 4, S3) (6,8). The time between visual symptom onset and MRI examination affects the sensitivity, with the optimal threshold for detecting restricted diffusion being 5 days (7). Distinguishing arteritic anterior ION from nonarteritic anterior ION is essential, as early treatment with corticosteroids in giant cell arteritis minimizes the risk of vision loss.

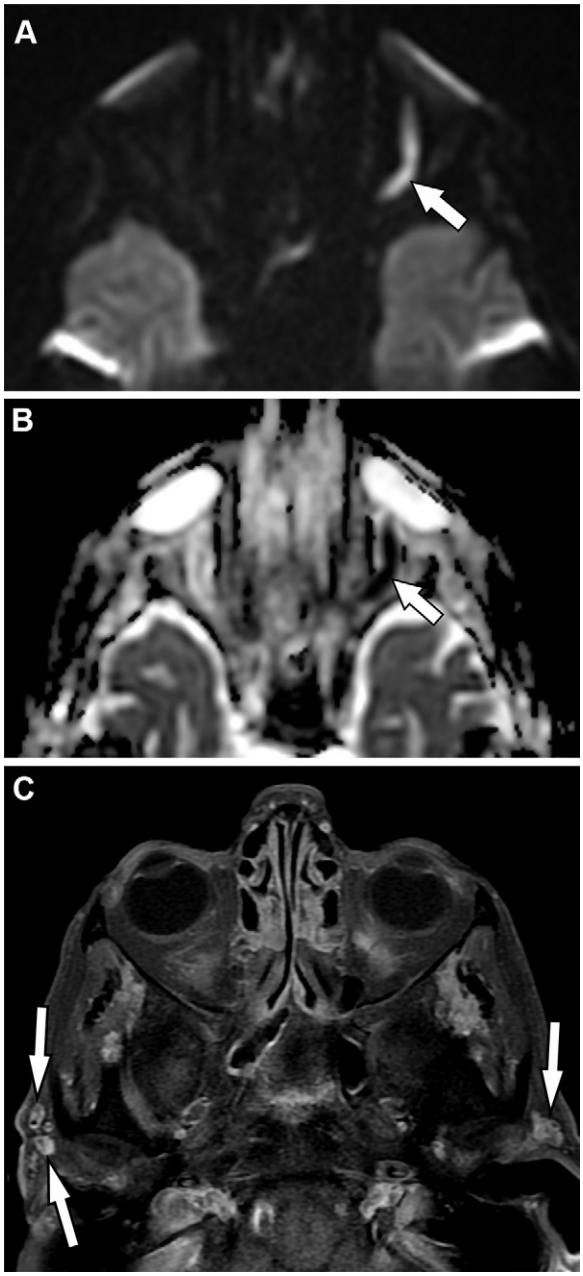

Figure 4. Posterior ION in a 82-year-old man with a history of new subacute headache who presented with sudden left vision loss. **(A)** Axial diffusion-weighted MR image shows restricted diffusion affecting the posterior intraorbital segment of the left optic nerve (arrow). **(B)** Axial apparent diffusion coefficient map confirms the restricted diffusion (arrow). **(C)** Additional axial contrast-enhanced three-dimensional T1-weighted vessel wall MR image shows marked bilateral superficial temporal artery enhancement and wall thickening, consistent with temporal arteritis (arrows).

Optic Nerve Gliomas

Optic nerve gliomas are the most common primary neoplasms of the optic nerve. The majority of these tumors are

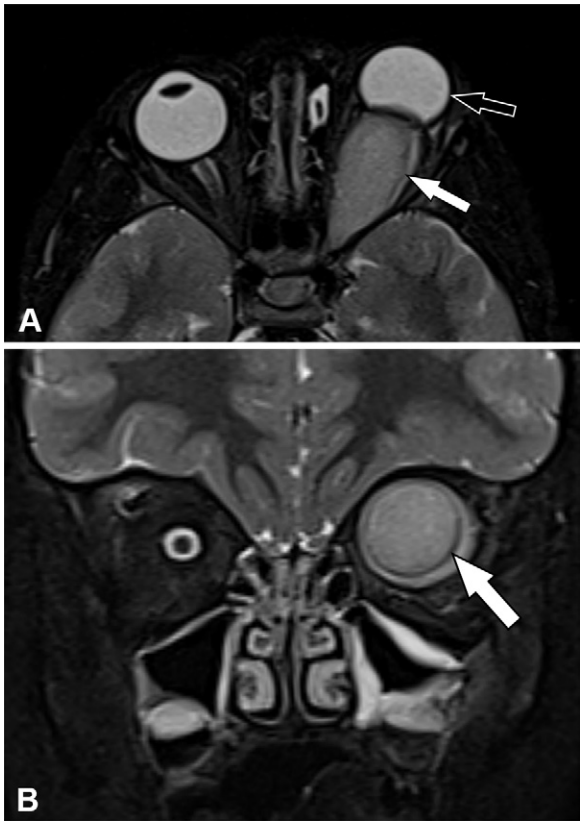

Figure 5. Sporadic optic nerve glioma in a 3-year-old girl. **(A)** Axial fat-saturated T2-weighted MR image shows an expansive lesion indistinguishable from the left optic nerve (white arrow) with predominantly hyperintense and heterogeneous signal intensity relative to the contralateral nerve,leading to proptosis (black arrow). **(B)** Coronal fat-saturated T2-weighted MR image shows an expansive lesion centered at the optic nerve (arrow).

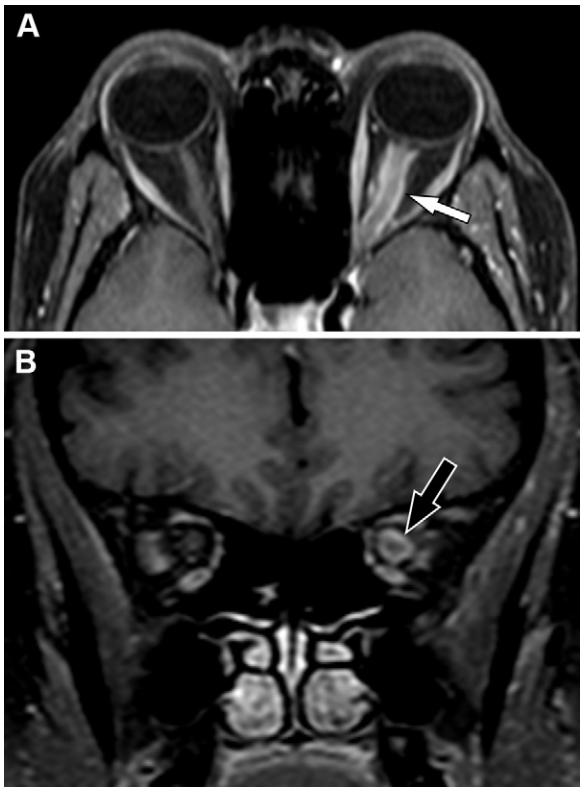

Figure 6. Optic nerve sheath meningioma in a 48-year-old woman who presented with left progressive vision loss. **(A)** Axial gadolinium-enhanced fat-saturated T1-weighted MR image shows the tram-track sign (arrow) on the left ONSC characterized by homogeneous enhancement of the nerve sheath surrounding the nonenhancing optic nerve. **(B)** Coronal gadolinium-enhanced fat-saturated T1-weighted MR image shows doughnut sign due to enhancing optic nerve sheath meningioma (arrow).

low-grade astrocytomas and are predominantly found in the pediatric population. Optic nerve gliomas are associated with a diagnosis of neurofibromatosis type 1 (NF1), and bilateral optic nerve gliomas are pathognomonic for this condition (9). In contrast, adults may present with more aggressive forms, such as high-grade astrocytoma (10,11).

At MRI, optic nerve glioma typically appears as nerve enlargement, with isointense signal at T1-weighted imaging and isointense-hyperintense signal at T2-weighted imaging relative to the contralateral nerve. Contrast enhancement is frequently minimal or absent. The tumor is indistinguishable from the nerve itself, a relevant distinction from meningiomas, which are associated with neurofibromatosis type 2 (NF2) (12).

NF1-associated gliomas are characterized by optic nerve enlargement and increased tortuosity (Fig S4). A peripheral rim of T2 hyperintensity is often evident around the nerve, associated with an expanded dural sheath and subarachnoid myxomatous tissue. Lesions in patients without NF1 (sporadic glioma) tend to manifest with masslike nerve enlargement, possibly with cystic components (Fig 5) (10,13,14).

Optic Nerve Sheath Meningioma

Optic nerve sheath meningioma is an uncommon benign neoplasm originating from the meningothelial cells of the meninges surrounding the optic nerve, the sole cranial nerve possessing meningeal coverings. Primary optic nerve sheath meningioma most often affects the intraorbital and intracanalicular nerve segments (10,14,15).

Patients typically present with unilateral painless progressive visual loss with optic nerve atrophy at fundoscopy. Average age at presentation is during the 4th or 5th decade of life (10,15). Imaging findings include segmental or diffuse nerve thickening, most commonly tubular thickening, but can also display a globular or fusiform morphology. Intratumoral calcification is common. The key suggestive finding is homogeneous tumoral enhancement (10,15). At axial or sagittal imaging, the enhancing tumor surrounding the optic nerve results in the "tram-track" sign (Fig 6).

Optic Perineuritis

Optic perineuritis is an inflammatory disorder that affects the optic nerve sheath. Optic perineuritis is most frequently caused by idiopathic orbital inflammatory disease and is described as primary optic perineuritis. However, it can also occur secondary to autoimmune and infectious diseases, including vasculitis and sarcoidosis (16).

Clinical findings may resemble those of optic neuritis, manifesting with subacute unilateral periorbital pain exacerbated

Figure 7. Idiopathic optic perineuritis in a 48-year-old man who presented with right vision loss and painful eye movement. Coronal gadolinium-enhanced fat-saturated T1-weighted MR image shows right optic nerve sheath contrast enhancement (arrow), accompanied by adjacent fat enhancement, while the optic nerve itself remains preserved.

by eye movement, vision loss, and optic disc edema. In contrast, perineuritis is associated with longer progression, over 2 weeks, without spontaneous improvement and affects older patients (16). Characteristic imaging features include linear enhancement of the optic nerve sheath, accompanied by infiltration of the intraconal fat with relative sparing of the optic nerve. (Fig 7) (1,16).

Intraconal Space

The intraconal space houses fat, orbital vessels, and cranial nerves, primarily motor nerves responsible for ocular motility. Pathologically, vascular lesions are most commonly observed within this space.

Vascular Malformations

Orbital vascular lesions can be classified into vascular tumors and malformations based on origin (17). Tumors are characterized by a proliferating endothelium, whereas malformations arise from developmental errors in angiogenesis. Malformations can affect arterial, venous, or lymphatic vessels and can consist of these elements alone or in combination.

Cavernous venous malformation (CVM), previously called cavernous hemangioma, is the most common benign orbital mass in adults. CVMs are nondistensible encapsulated masses containing dilated venous blood vessels. The lateral retrobulbar intraconal space is the most common location for CVM, while the orbital apex and extraconal space are less frequently affected. CVMs occur more often in middle-aged women and manifest with slowly progressive painless proptosis. Larger lesions can cause functional symptoms such as impaired vision and diplopia (18). CVM in the orbital apex can produce visual loss due to optic nerve compression even at a small size, with minimal proptosis.

Imaging features include ovoid well-defined masses with soft-tissue attenuation at CT and potentially phleboliths. Adjacent bone remodeling is a prominent feature of CVMs and other benign lesions, indicating slow growth, which contrasts with bony erosion observed in aggressive lesions. At MRI, lesions exhibit isointensity on T1-weighted images and hyperintensity on T2-weighted images to adjacent EOMs. Internal septations and a fibrous pseudocapsule appear as hypointensity on T2-weighted images (18–20). A progressive enhancement pattern is a characteristic finding of CVMs, exhibiting initial poor and heterogeneous central enhancement on CT and MR images, with subsequent filling and homogeneous intensity on delayed images (Fig 8) (20).

Venous malformations, frequently referred to as orbital varices, are abnormal venous networks with variable connections to the systemic venous circulation. Systemic connections are evidenced by distention of lesions when venous pressure increases (during the Valsalva maneuver), which can be observed clinically as reversible proptosis. Acute presentations due to thrombosis or hemorrhage manifest as sudden painful edema, ecchymosis, or sustained proptosis (21–23).

Venous malformations commonly occur within the intraconal space, manifesting as fusiform or teardrop-shaped lesions that are often contiguous with the superior or inferior ophthalmic veins. Imaging features include distensible lesion during the Valsalva maneuver, intralesional phleboliths, and avid contrast enhancement (Fig 9). At MRI, venous malformations exhibit homogeneous hypointensity-isointensity on T1-weighted images and hyperintensity on T2-weighted images. Areas of hyperintense signal intensity on T1-weighted images may indicate hemorrhage or thrombosis, while hypointense foci on both T1- and T2-weighted images are associated with thrombi or phleboliths.

Lymphatic malformations (LMs) consist of anomalous lymphatic spaces formed by a nonfunctional network of cystic structures filled with serous fluid. Typically, patients with LMs are diagnosed during early childhood. Deep LMs most commonly manifest with acute enlargement due to inflammation or bleeding, resulting in painful proptosis, restricted ocular motility, and visual impairment. Some LMs maintain relative stability, leading to progressive proptosis (21,24).

At MRI, LMs are often transpatial lesions, manifesting primarily as macrocysts (>1 cm), microcysts (<1 cm), or with mixed composition. Cystic signal intensity is variable depending on the presence and age of hemorrhagic components. Fluid-fluid levels are a characteristic finding, indicating recent intralesional hemorrhage (Fig 10). Although LMs typically do not exhibit contrast enhancement, the venous components in a venolymphatic malformation will enhance, allowing differentiation between the lymphatic and venous parts of the lesion.

Orbital Metastasis

Metastatic tumors account for up to 13% of all orbital tumors. The orbit is an uncommon site for hematogenous spread and is associated with advanced disease and poor prognosis (25,26). The most common tumor that metastasizes to the orbit is breast cancer, followed by melanoma, prostate, and lung cancer (26). The most common symptoms are progressive proptosis, orbital swelling, pain, and diplopia. Enophthalmos is a paradoxical feature observed in sclerotic or scirrhous tumors, such as breast and gastrointestinal metastases, resulting from orbital fat contraction due to desmoplasia and fibrosis (26). In patients with a previous history of cancer and a new orbital mass, metastatic disease should be considered.

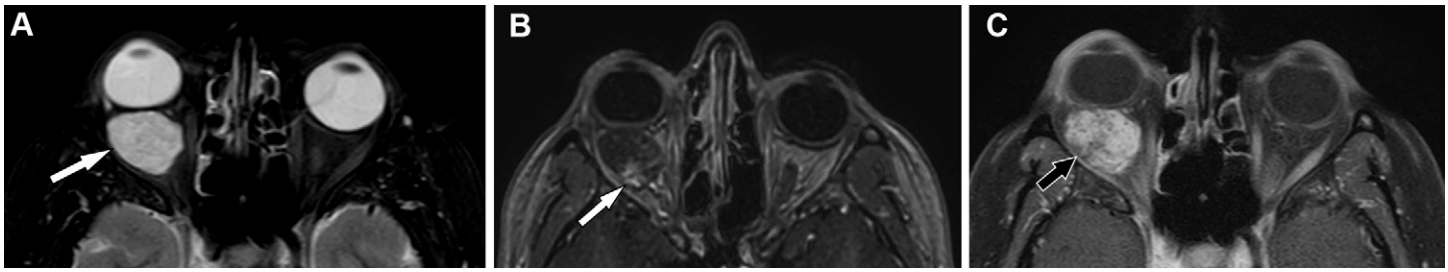

Figure 8. CVM in a 43-year-old man who presented with right proptosis. **(A)** Axial fat-saturated T2-weighted MR image shows a well-circumscribed intraconal lateral retrobulbar mass (arrow) with high signal intensity and a peripheral low signal intensity capsule, resulting in anterior displacement of the globe. **(B)** Axial early-phase gadolinium-enhanced fat-saturated T1-weighted MR image 120 seconds following contrast administration shows mild central enhancement (arrow). **(C)** Axial delayed phase MR image 390 seconds following contrast administration shows progressive filling enhancement (arrow).

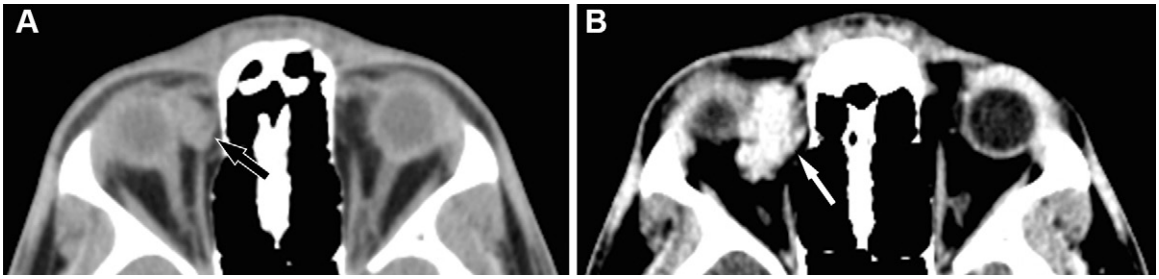

Figure 9. Orbital varix in a 56-year-old man. **(A)** Axial nonenhanced CT image shows a well-circumscribed intraconal lesion (arrow) in the right orbit with soft-tissue attenuation, originally measuring 1.4 × 0.6 cm. **(B)** Axial contrast-enhanced CT image obtained during the Valsalva maneuver shows that the lesion (arrow) enlarged to 2.8 × 1.2 cm, with avid enhancement, causing lateral and inferior displacement of the globe. The observed change in size aids in the differential diagnosis from other vascular malformations.

Figure 10. Orbital venolymphatic malformation in a 7-year-old boy who presented with right proptosis and diplopia. Axial fat-saturated T2-weighted MR image shows a multicystic lesion in the right orbit, crossing anatomic boundaries and affecting both the periorbital and orbital regions. Within the orbit, the lesion extends into both the intra- and extraconal compartments, exhibiting characteristic fluid-fluid levels, indicative of recent intralesional bleeding (arrow).

Orbital metastases are multicompartmental, potentially infiltrating fat and EOMs. Imaging findings range from a well-defined focal lesion to an ill-defined diffuse infiltrative pattern with loss of orbital anatomic landmarks and heterogeneous contrast enhancement (Figs 11, S5) (25).

Conal Space

The conal space is delineated by the EOMs, which converge at the orbital apex. The four recti muscles form a tendinous ring, the annulus of Zinn, surrounding the optic canal containing the optic nerve and ophthalmic artery (Fig 1). Most of the EOMs are innervated by the oculomotor nerve, except for the superior oblique (trochlear nerve) and lateral rectus (abducens nerve) muscles. Diplopia and strabismus are common symptoms related to conal pathologic conditions, which may result from restrictive motility due to mechanical compression or EOM enlargement (27).

Thyroid Eye Disease and Graves Orbitopathy

Thyroid eye disease (TED) is an autoimmune disorder of the orbital tissue that is associated with dysthyroidism, most commonly Graves disease and hyperthyroidism, but it can also manifest in individuals with hypothyroidism or euthyroidism due to Hashimoto disease. Myopathic TED exhibits a biphasic course: a self-limited active phase with progressive symptoms and inflammatory changes, followed by an inactive phase with residual symptoms (28). Identifying patients in the active phase allows for targeted treatment improving disease prognosis.

TED is characteristically bilateral and symmetric. EOM involvement results in restricted ocular motility, manifesting as diplopia and strabismus. Other common symptoms include eyelid retraction and proptosis. Active disease is suggested by inflammatory symptoms such as orbital pain, eyelid edema, and erythema. Elevated levels of thyroid-stimulating

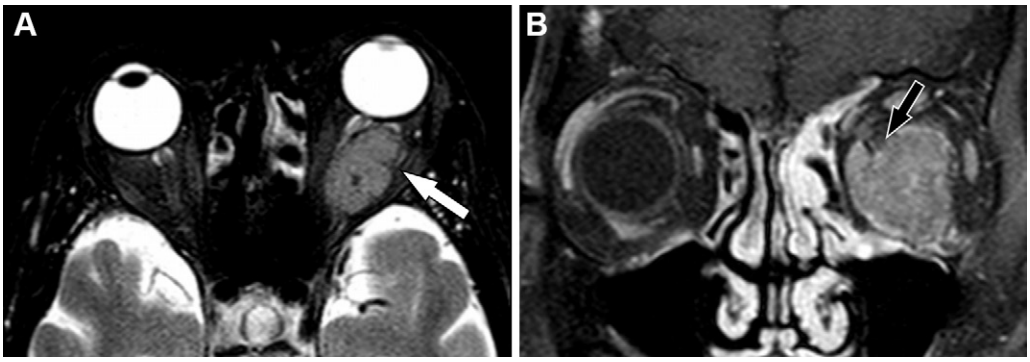

Figure 11. Metastasis in a 59-year-old man with a history of prostate cancer who presented with left-sided proptosis and vision loss. **(A)** Axial fat-saturated T2-weighted MR image shows an intraconal infiltrative mass predominantly with intermediate signal intensity (arrow). **(B)** Coronal gadolinium-enhanced fat-saturated T1-weighted MR image highlights optic nerve infiltration (arrow) and mass enhancement.

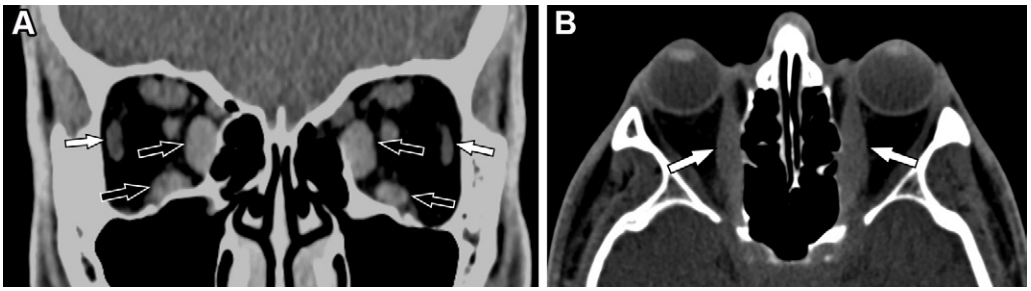

Figure 12. Graves orbitopathy in a 33-year-old man with bilateral proptosis. **(A)** Coronal unenhanced CT image illustrates bilateral and symmetric EOM thickening predominantly affecting the inferior and medial rectus (black arrows), with a relatively spared lateral rectus (white arrows). **(B)** Axial unenhanced CT image shows the Coca-Cola bottle sign (arrows), characterized by fusiform enlargement of the affected medial rectus with sparing of the tendinous insertions.

hormone receptor binding antibodies (TRAbs), free thyroxine (T4), and triiodothyronine (T3) are the most frequent laboratory findings (29,30).

Imaging features include muscle enlargement sparing the tendinous insertions, appearing as fusiform muscle enlargement ("Coca-Cola bottle" sign), increased orbital fat volume, and lacrimal gland enlargement (29,31). Findings suggestive of active disease include acute muscle enlargement and signs of edema, the most reliable being hyperintensity on T2-weighted images (32,33). In inactive disease, the EOMs remain enlarged due to osmotic edema but display fibrosis and fatty infiltration.

The involvement of EOMs in TED typically affects multiple muscles and follows a characteristic pattern: the *i*nferior rectus is most frequently affected, followed by *m*edial rectus, *s*uperior rectus, *l*ateral rectus, and *o*blique muscles ("I'M SLOw" mnemonic) (Fig 12). Severe EOM thickening in the orbital apex can lead to direct compression of the optic nerve, manifesting as deterioration of central vision. Imaging can be used to confirm clinically suspected cases in the presence of apical crowding or significant nerve stretching (Fig S6) (30,33,34). TED is the most common cause of EOM enlargement. However, other causes should be considered in the presence of atypical features, including unilateral enlargement, atypical muscle pattern, involvement of adjacent structures, restricted diffusion, and absence of pain (31).

Idiopathic Orbital Inflammation

Idiopathic orbital myositis is an inflammatory process of unknown cause involving the EOMs and is a subtype of idiopathic orbital inflammation. Furthermore, idiopathic orbital inflammation can manifest with dacryoadenitis, optic perineuritis, and focal masses. Among these subtypes, myositis and dacryoadenitis are the most prevalent (35,36).

The disease pathophysiology is unclear but is believed to be linked to an autoimmune process. Histopathologic studies revealed chronic inflammatory cellular infiltrates with varying degrees of fibrosis (36). Clinically, the typical manifestation includes acute or subacute diplopia with orbital edema, erythema, proptosis, and orbital pain exacerbated by eye movement. Unilateral involvement and response to corticosteroids are characteristic, but bilateral, chronic, or recurrent cases are not rare (35,37).

The most frequently involved muscle is the medial rectus, followed by the lateral, superior, and inferior rectus (35,37). Imaging shows homogeneous enlargement of the EOMs, frequently involving the tendinous insertions, resulting in a tubular morphology. Concurrent inflammatory changes may occur in the fat bordering the muscle, blurring the muscle margin. At MRI, involved muscles exhibit contrast enhancement. At T2-weighted imaging, components within the muscle that exhibit hyperintensity suggest active inflammation, while areas with hypointense signal intensity are indicative of fibrosis (Fig 13) (37,38).

Immunoglobulin G4–related Disease

Immunoglobulin G4 (IgG4)–related disease is a multisystemic immune-mediated condition characterized by lymphoplasmacytic tissue infiltration with an abundance of IgG4 plasma cells and fibrosis. It commonly affects the orbit (IgG4-related opthalmic disease [IgG4-ROD]), involving the lacrimal gland

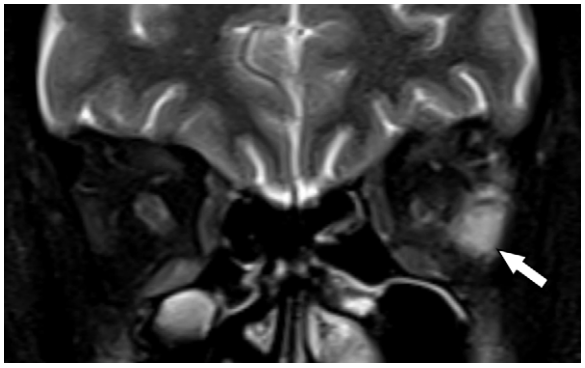

Figure 13. Idiopathic orbital myositis in a 33-year-old woman who presented with left abduction restriction in the left eye. Coronal fat-saturated T2-weighted MR image shows enlargement and increased signal intensity of the lateral rectus muscle (arrow) accompanied by adjacent fat stranding. Unilateral manifestation and initial involvement of the lateral rectus are atypical for TED, suggesting an alternative diagnosis.

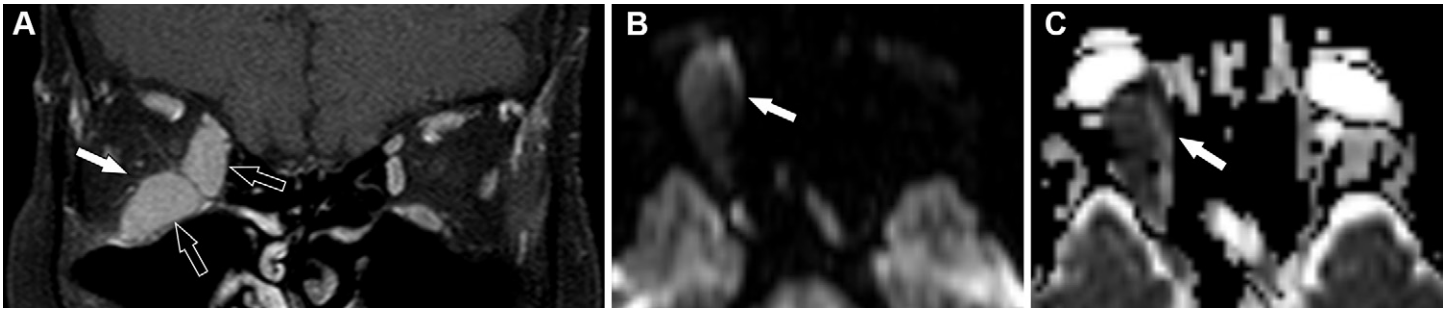

Figure 14. Conal lymphoma in a 60-year-old woman who presented with right proptosis and restricted ocular motility. **(A)** Coronal gadolinium-enhanced fat-saturated T1-weighted MR image shows unilateral muscle enlargement affecting the inferior and medial rectus with homogeneous enhancement (black arrows) and relatively preserved surrounding fat (white arrow). **(B, C)** Axial diffusion-weighted MR image **(B)** and apparent diffusion coefficient map **(C)** show marked restricted diffusion in the medial rectus (arrow), a finding suggestive of a neoplastic cause, specifically lymphoma. An orbital biopsy confirmed the diagnosis.

and EOM most frequently (39). Clinical features include painless periorbital swelling, proptosis, diplopia, and restricted eye motility with a subacute or chronic course. Elevated serum IgG4 levels, while a supporting feature, may not always be present. Orbital involvement is typically bilateral but potentially asymmetric (39,40).

In contrast to TED and idiopathic orbital inflammation, EOM involvement in IgG4-ROD is often disassociated from muscular function, as markedly enlarged lesions exhibit discrete clinical signs of ocular restriction (41).

Imaging findings include homogeneous muscle enlargement, tendinous sparing, and adjacent fat stranding due to inflammation. At MRI, affected muscles display increased enhancement and intermediate or low signal intensity on T2-weighted images, attributed to increased cellularity or fibrosis. Occasionally, scattered high T2-weighted signal intensity suggests acute inflammation. A single muscle or multiple muscles may be involved, with the lateral rectus being the most commonly affected. This contrasts with TED, where lateral rectus enlargement is a late manifestation. Additional manifestations include lacrimal gland and cranial nerve enlargement, particularly branches of the trigeminal nerve; orbital fat infiltration, potentially resulting in a focal mass; and a greater incidence of paranasal mucosal thickening (Fig S7) (31,39,40).

Neoplastic Conditions

Metastases and lymphomas centered in the EOMs are uncommon; typically, muscular involvement arises from infiltration by an adjacent mass (31,42). Clinical features include proptosis, diplopia, and motility disturbances. Pain is characteristically absent in lymphomas but potentially present with metastases (42–44). Imaging findings aid in distinguishing these conditions from other causes of muscle enlargement, with restricted diffusion being a key indicator (31,45). Lymphoma mainly manifests unilaterally with fusiform muscle enlargement, possibly involving the tendons. Lesions exhibit diffuse homogeneous enhancement and very low apparent diffusion coefficient (Fig 14). Metastases typically manifest as either a focal mass or diffuse muscle infiltration, with irregular margins and increased enhancement (Fig S8) (42–46).

Extraconal Space

The extraconal space contains fat, blood vessels, and nerve branches, which are primarily sensory branches of cranial nerves. Pathologically, the extraconal space exhibits a higher incidence of schwannomas, as well as inflammatory and infiltrative lesions such as cellulitis and lymphoma.

Infection

Infectious disease of the orbit is the most frequent primary orbital pathologic condition. While bacterial pathogens are the most common cause of orbital infections, invasive fungal causes should be considered in patients who are immunocompromised or have diabetes mellitus. Distinguishing between preseptal and postseptal infection is important for patient management since postseptal infection can result in vision loss and intracranial infection. The orbital septum, a

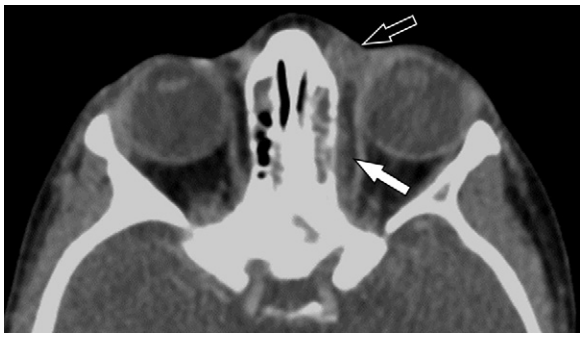

Figure 15. Orbital and periorbital cellulitis in a 5-year-old girl who presented with left orbital pain and restricted ocular motility. Axial contrast-enhanced CT image shows left orbital fat straining (white arrow) in the extraconal compartment, adjacent to ethmoidal sinusitis, indicating orbital cellulitis, along with a linear subperiosteal collection. Additionally, there is a fat straining of the periorbital soft tissues (black arrow).

fibrous sheet extending from the orbital rim to the eyelids, serves as a barrier to prevent infection spread.

Preseptal or periorbital cellulitis is an infection limited to the skin and soft tissues anterior to the orbital septum, often associated with local trauma, such as a bug bite, or contiguous spread from dental or sinus infections. Postseptal or orbital cellulitis affects soft tissues posterior to the orbital septum, most frequently due to contiguous spread from a sinus infection. Other causes include trauma and spread from dental and preseptal infections.

Common clinical features include swelling and erythema of the eyelid. Proptosis, vision impairment, and ophthalmoplegia suggest postseptal infection. CT of the orbits is the preferred method for evaluating orbital infection. Preseptal cellulitis appears as periorbital soft-tissue swelling anterior to the orbital septum. In contrast, postseptal infection manifests as soft-tissue stranding posterior to the orbital septum, potentially associated with EOM thickening and lacrimal gland enlargement (Fig 15) (47–49).

Orbital and subperiosteal abscesses are the most common complications of postseptal cellulitis. These abscesses typically manifest with fluid collection and peripheral enhancement. Subperiosteal abscesses are mostly derived from ethmoidal sinus infections, forming a lentiform-shaped collection within the subperiosteal space along the medial orbital wall (47,50).

Infantile Hemangioma

Infantile hemangiomas (IHs) are common benign neoplasms that occur during infancy. These lesions are characterized by lobules of vasoformative endothelial proliferation, resulting in nonencapsulated masses (17,51,52). IHs undergo a rapid growth phase during the first 5 months, followed by a slow growth phase and a characteristic involution phase, most often starting at approximately 1 year of age and lasting for several years (53).

Preseptal IHs can be identified by skin lesions such as red strawberry marks or eyelid edema. Deep orbital lesions are associated with proptosis and occasionally causing ocular restriction (51,52). Imaging is reserved for atypical or deep IHs. Lesions are typically extraconal and well defined with lobulated contours. Phleboliths are not present in IHs, aiding in the differential diagnosis of vascular lesions. At MRI, early proliferative IHs appear isointense on T1-weighted images and hyperintense on T2-weighted images compared with adjacent EOMs and exhibit marked homogeneous enhancement. High-flow feeding vessels inside or along the lesion are characteristic, exhibiting low signal intensity due to flow voids (Fig 16). In the involutional phase, progressive fat deposition occurs, resulting in increased signal intensity on both T1- and T2- weighted images associated with signs of fibrosis, indicated by decreased T2 signal intensity (21,51).

Rhabdomyosarcoma

Rhabdomyosarcoma is the most common mesenchymal tumor in children. Contrary to early belief, these tumors do not arise from EOMs but from primitive mesenchymal cells that differentiate into striated muscle cells, making them more common in the extraconal space and not always centered within the EOMs. The most prevalent subtypes in the orbit are embryonal, manifesting in childhood, and alveolar, typically occurring in older children and young adults (54). Patients present with rapidly developing unilateral proptosis and swelling of the conjunctiva and eyelid (54,55).

Orbital rhabdomyosarcoma behaves aggressively, frequently displaying adjacent bone erosion. If the tumor invades orbital bones or the optic nerve, it is classified as parameningeal, which is associated with a worse prognosis. At cross-sectional imaging, most lesions are homogeneous with diffuse enhancement. Early lesions may have circumscribed margins, while larger tumors are ill-defined. Necrosis and hemorrhage are uncommon findings. At MRI, rhabdomyosarcoma manifests with isointense signal on T1-weighted images and hyperintense signal on T2-weighted images to adjacent EOMs (54,55). Restricted diffusion is a characteristic finding distinguishing rhabdomyosarcoma from lesions with similar features, such as IH (Fig 17) (56,57).

Nerve Sheath Tumor

Schwannomas are benign peripheral nerve sheath tumors originating from Schwann cells. Orbital schwannomas most commonly arise from sensory nerves, particularly the supraorbital and supratrochlear nerves extraconal branches of the ophthalmic trigeminal nerve (V1). Orbital schwannoma can also manifest as an intraconal tumor, frequently derived from the nasociliary nerve (V1) (57). Clinical features include painless progressive proptosis, eyelid swelling, and/or a palpable mass. Due to their frequent location in the superior orbit, patients may present with hypophthalmos (58,59).

At imaging, orbital schwannomas are well-defined masses generally aligned with the long axis of the involved nerve. Lesions can mold to the surrounding structures, appearing cone-shaped when involving the orbital apex or dumbbell-shaped when involving orbital fissures. At MRI, tumors can be homogeneous or heterogeneous according to their variable histologic composition. Antoni A, compact cellular areas, are associated with isointensity-hypointensity at T2-weighted imaging and increased contrast enhancement,

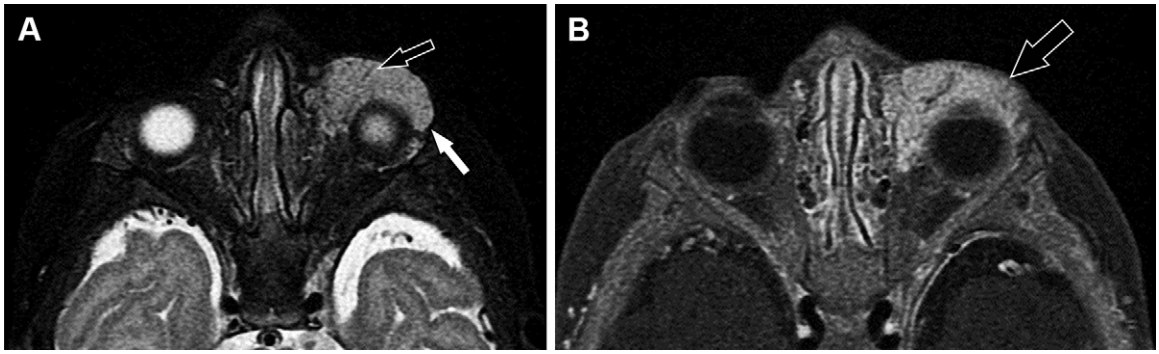

Figure 16. IH in a 6-month-old girl. **(A)** Axial fat-saturated T2-weighted MR image shows lobulated expansive lesion (white arrow) involving the left periorbital and orbital regions, affecting the extraconal and intraconal spaces, exhibiting hyperintense signal with small hypointense flow voids (black arrow). **(B)** Axial gadolinium-enhanced fat-saturated T1-weighted MR image shows intense enhancement (arrow).

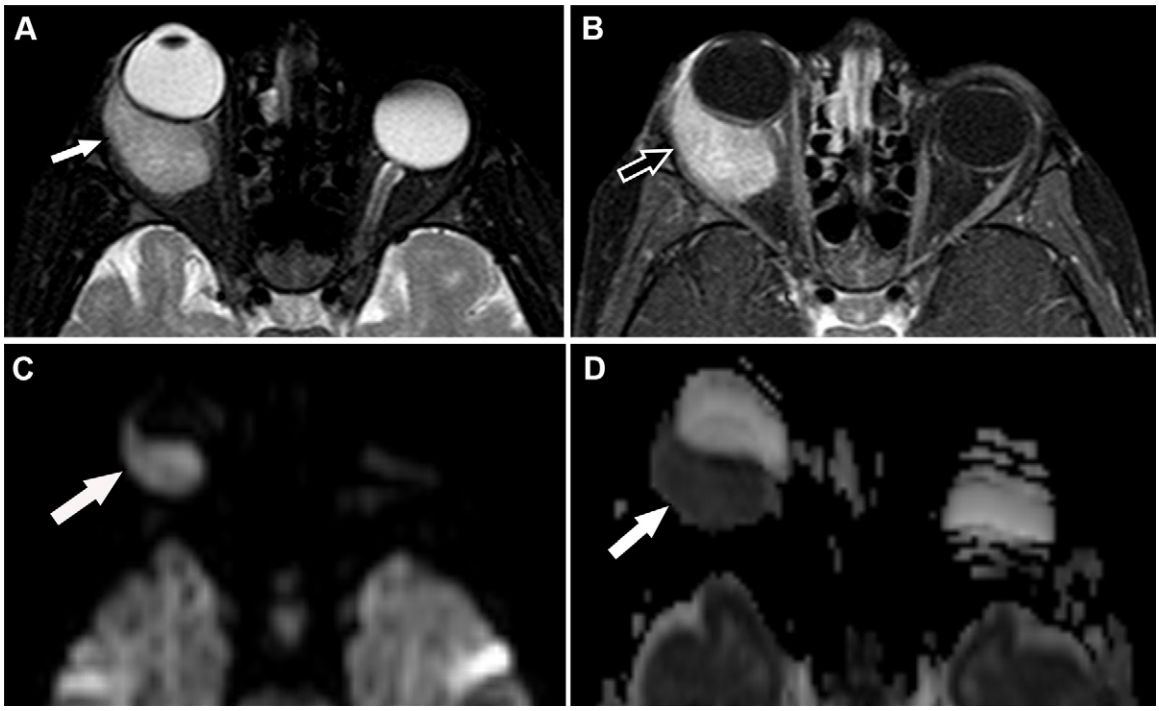

Figure 17. Rhabdomyosarcoma in a 5-year-old girl who presented with right palpebral swelling and proptosis. **(A)** Axial fat-saturated T2-weighted MR image shows an invasive expansive lesion with hyperintense signal (arrow) affecting both the extraconal and intraconal compartments of the right orbit, resulting in anterior displacement of the globe. **(B)** Axial gadolinium-enhanced fat-saturated T1-weighted MR image shows avid enhancement of the lesion (arrow). **(C, D)** Axial diffusion-weighted MR image **(C)** and apparent diffusion coefficient map **(D)** shows restricted diffusion (arrow), suggestive of malignancy.

while regions of lower cellular density, Antoni B, are associated with hyperintensity at T2-weighted imaging (60). Typically, schwannomas exhibit isointensity compared with EOMs on T1-weighted images and heterogeneous hyperintensity on T2-weighted images with heterogeneous contrast enhancement (Fig 18). Other possible manifestations include homogeneous isointense-hypointense signal at T2-weighted imaging with marked enhancement and multicystic lesions with enhancement restricted to solid portions (57,60,61).

In the intraconal space, schwannomas can exhibit features reminiscent of cavernous malformations. The contrast spread pattern at dynamic imaging is the most reliable feature for differentiating between these lesions. CVMs demonstrate progressive enhancement, whereas schwannomas exhibit immediate enhancement (Fig S9) (20).

Neurofibromas are benign peripheral nerve tumors composed of Schwann cells and nonneoplastic components. Like schwannomas, neurofibromas are frequently extraconal and are derived from sensory nerves. Differentiating neurofibromas from schwannomas might not always be possible. A patient's clinical history can suggest a diagnosis. Plexiform neurofibroma is characteristic of NF1 while multiple schwannomas are associated with NF2. At MRI, neurofibromas can manifest with a hyperintense rim surrounding a central

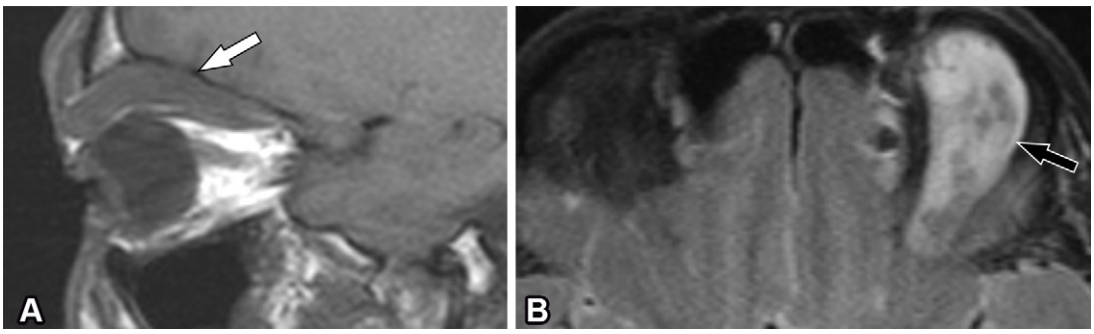

Figure 18. Orbital schwannoma in a 40-year-old man with left eyelid swelling and a palpable mass. **(A)** Sagittal T1-weighted MR image shows an expansive lesion with an elongated anteroposterior morphology in the superior extraconal compartment, affecting the left orbit (arrow). **(B)** Axial fat-saturated T2-weighted MR image shows a well-defined heterogeneous lesion with predominantly hyperintense signal intensity (arrow). The signal intensity characteristics at this typical location were considered suggestive of schwannoma, a diagnosis that was subsequently confirmed with orbital biopsy.

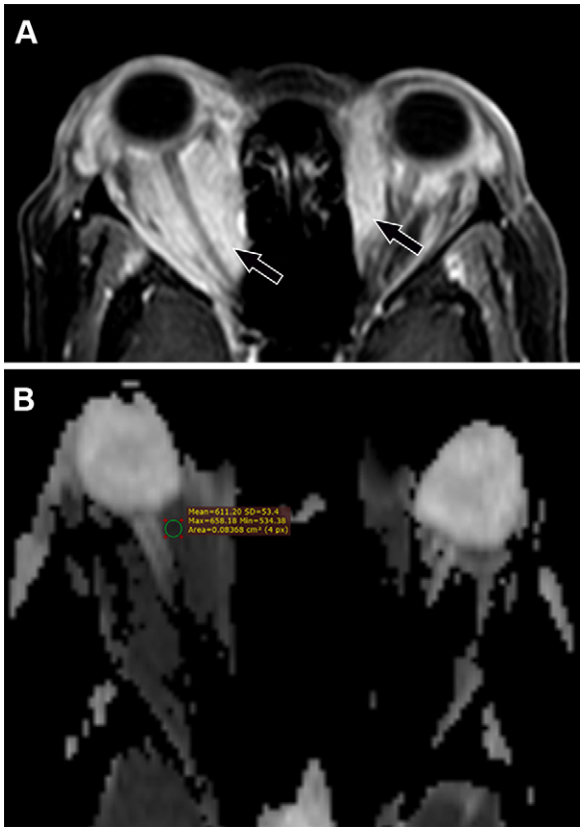

Figure 19. Orbital lymphoma in a 57-year-old woman who presented with bilateral proptosis and ocular restricted motility. **(A)** Axial gadolinium-enhanced fat-saturated T1-weighted MR image shows infiltrative expansive multicompartmental lesions with homogeneous enhancement, involving the extraconal and intraconal compartments in both orbits (arrows). **(B)** Axial apparent diffusion coefficient map with a region of interest placed within the mass shows a mean value of 611 × 10^{-6} mm^2/sec, suggestive of a malignant lesion (particularly lymphoma) indicated by the very low apparent diffusion coefficient value. An orbital biopsy confirmed the diagnosis.

hypointense area on T2-weighted images ("target" sign), whereas schwannomas commonly manifest with central hyperintensity surrounded by hypointensity on T2-weighted images due to hemorrhagic or cystic degeneration (12,57–60).

Lymphoproliferative Disorders

Lymphoproliferative lesions include a spectrum of disorders, including lymphoid hyperplasia, atypical lymphocytic infiltrate, and malignant lymphoma (62). These lesions are common causes for primary orbital tumors in adults, with malignant lymphoma being the most represented. The majority of patients have B-cell non-Hodgkin lymphoma, particularly extranodal marginal zone lymphoma. Malignant lesions originate from reactive lymphoid tissue acquired by persistent antigenic stimulation, associated with other factors related to genetic instability (46,63). Clinical features include proptosis, limited eye motility, and changes in visual acuity. Pain is an infrequent symptom. Most cases manifest with unilateral orbital involvement in the 5th to 7th decades of life (46,63).

Lymphoproliferative lesions can affect any anatomic space, with the extraconal space being the most involved (46). At imaging, tumors can appear as either diffuse ill-defined or round circumscribed masses. Lesions tend to mold to surrounding orbital structures, and continuous growth may result in bone remodeling. Bone erosion is not typical but can occur in higher-grade lymphomas. At MRI, most lesions are isointense compared with EOMs at both T1-weighted imaging and T2-weighted imaging with homogeneous enhancement (46,62). Low T2 signal intensity is generally observed in lymphoma and is related to a high cell density. Lymphomas frequently exhibit very low apparent diffusion coefficient values, with a proposed threshold of less than 612 × 10^{-6} mm^2/sec (56,64) (Fig 19).

Lacrimal Apparatus

The lacrimal apparatus comprises the lacrimal glands, lacrimal sacs, and ducts. The lacrimal gland is located in the superolateral extraconal space. It can be anatomically divided into an orbital lobe and a palpebral lobe, separated by the aponeurosis of the levator palpebrae muscle (Fig 1A). The orbital lobe, which is larger and posterior to the aponeurosis,

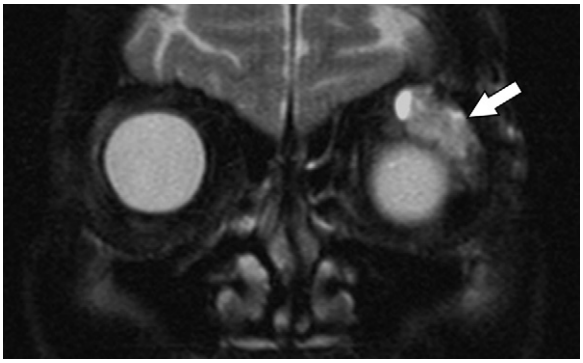

Figure 20. Pleomorphic adenoma in a 64-year-old woman who presented with left proptosis and diplopia. Coronal fat-saturated T2-weighted MR image shows a capsulated expansive lesion in the lacrimal fossa within the extraconal space, exhibiting predominantly hyperintense heterogeneous signal intensity (arrow), without evidence of restricted diffusion (not shown). The diagnosis was confirmed through an orbital biopsy.

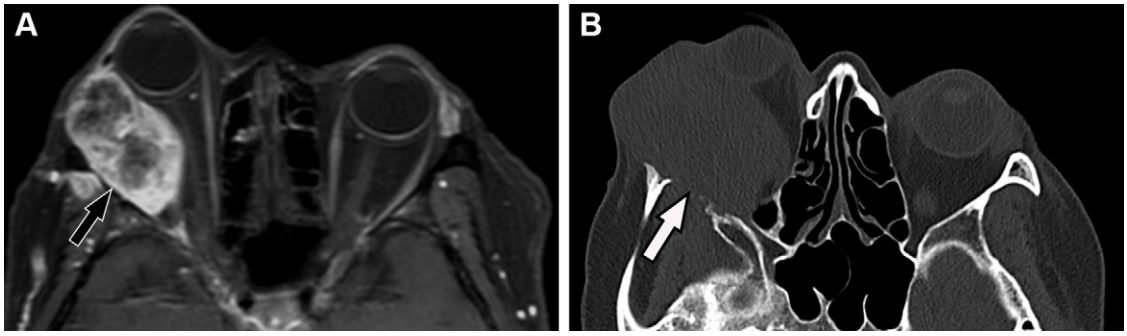

Figure 21. Adenoid cystic carcinoma in a 56-year-old woman who presented with right proptosis and pain. **(A)** Axial gadolinium-enhanced fat-saturated T1-weighted MR image shows an invasive expansive lesion involving the right lacrimal fossa (arrow) exhibiting heterogeneous enhancement and causing anteromedial displacement of the globe. **(B)** Axial nonenhanced CT image acquired 14 months after the initial MRI shows bone erosion in the lateral wall of the right orbit (arrow), indicative of malignancy. The diagnosis was confirmed through an orbital biopsy.

is the site of most epithelial neoplasms. Inflammatory and lymphoproliferative diseases generally exhibit a diffuse pattern, affecting both lobes.

Pleomorphic Adenomas

Pleomorphic adenomas, which are benign lesions with variable histologic compositions that contain both epithelial and mesenchymal tissue, are the most common tumors of the lacrimal gland (11,65,66). Patients present with a unilateral painless mass with or without proptosis. The presence of pain, sensory loss, and rapid growth are not typical and may suggest a more aggressive process.

Imaging shows a well-circumscribed round or oval lesion frequently found within the orbital lobe. Slow tumor growth may result in adjacent smooth bone scalloping. Small lesions are often homogeneous, while larger tumors can exhibit heterogeneity due to cystic degeneration. At MRI, pleomorphic adenomas typically exhibit T1 isointensity, T2 hyperintensity, and enhance following contrast media administration (Fig 20) (10,11,65,66).

Malignant Epithelial Tumors

The most prevalent subtypes are adenoid cystic carcinoma (most common); carcinoma ex pleomorphic adenoma, which arises from malignant transformation of a pleomorphic adenoma; and adenocarcinoma of the lacrimal glands. Malignant lacrimal tumors manifest with a firm unilateral painful mass with proptosis. They exhibit rapid infiltrative growth and a propensity for perineural spread, resulting in periorbital pain and paresthesia (10,56,66).

At imaging, malignant tumors can exhibit round and well-defined margins in early stages, progressing to an irregular mass with invasive margins in advanced disease. Perineural invasion is frequent, characterized by abnormal nerve enhancement and thickening. Signs indicative of malignancy in a lacrimal tumor include bone erosion, poorly defined margins, and infiltrative disease (11,65,66). At MRI, tumors often appear hypointense on T1-weighted images and intermediate-hyperintense on T2-weighted images, showing heterogeneous enhancement and frequently demonstrating restricted diffusion (Fig 21) (11,65).

Dacryoadenitis

Dacryoadenitis refers to inflammation of the lacrimal gland resulting from infection, autoimmune disease, or idiopathic inflammation. Acute cases are often infectious in children and young adults, typically with a viral cause, and resolve within 4–6 weeks. Clinically, these cases manifest with unilateral or bilateral painful gland enlargement, erythema, and eyelid edema (65,66). Autoimmune and idiopathic dacryoadenitis can be acute or chronic and can be associated with multiple conditions, including sarcoidosis, Sjögren syndrome, IgG4-related disease, and idiopathic orbital inflammation (66). Clinical manifestation involves pain, redness, and swelling. However, a noninfectious cause should be considered in acute events lacking clear inflammatory symptoms and a relapsing-remitting course (67).

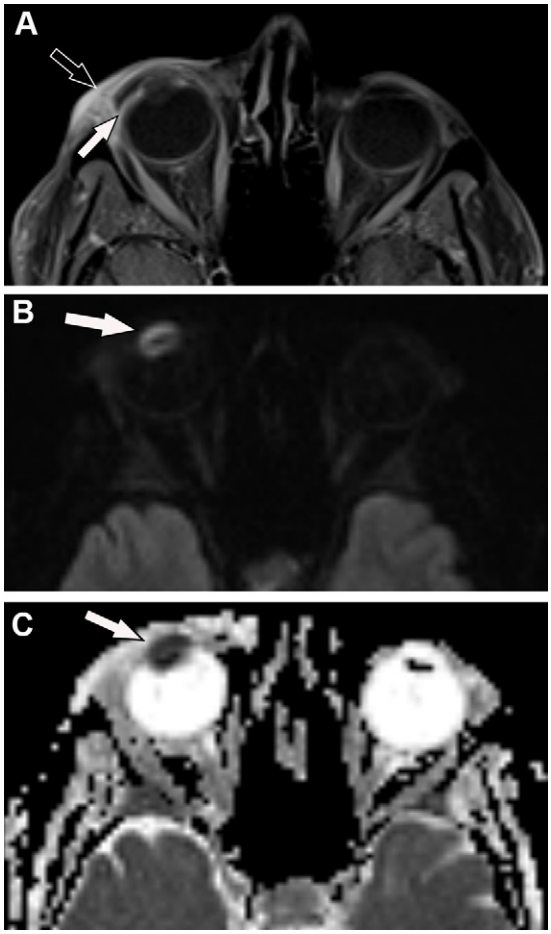

Figure 22. Endophthalmitis in a 53-year-old man who presented with right chemosis, orbital pain, and blurry vision and was previously treated for anterior uveitis. **(A)** Axial gadolinium-enhanced fat-saturated T1-weighted MR image shows thickening and enhancement of the uveal layer (white arrow) along abnormal signal intensity in the aqueous humor of the right globe. Dacryoadenitis and periorbital enhancement are noted, attributed to the extension of the inflammatory process (black arrow). **(B, C)** Axial diffusion-weighted MR image **(B)** and apparent diffusion coefficient map **(C)** show restricted diffusion in the aqueous humor, suggestive of purulent exudate (arrow).

At cross-sectional imaging, acute dacryoadenitis exhibits diffuse gland enlargement and periglandular soft-tissue straining. Marked enhancement can be observed at postcontrast imaging. Chronic dacryoadenitis manifests as unilateral or bilateral gland enlargement and moderate contrast enhancement. At MRI, the lacrimal gland exhibits isointensity-hypointensity on T1-weighted images and hyperintensity on T2-weighted images. Chronic inflammation in advanced stages is associated with fatty tissue replacement, gland atrophy, and fibrosis (65,66).

Lymphoproliferative Lesions

Lymphoproliferative disease in the lacrimal gland exhibits a clinical and histologic pattern consistent with that observed in the general extraconal space. Notably, involvement of the lacrimal gland is a marker for lymphoma, as well as development of systemic disease (62).

Imaging shows a well-circumscribed homogeneous mass or diffuse gland enlargement with substantial enhancement. At MRI, suggestive findings include diffusion restriction with low apparent diffusion coefficient values (Fig S10) (65,66). Patients with Sjögren syndrome are frequently followed due to their increased risk for lymphoma. In this setting, any substantial increase in gland size (68), lymphadenopathy, or restricted diffusion are important imaging markers.

Globe Compartment

The globe is continuous with the optic nerve and comprises three layers: the outer layer (sclera and cornea), the uveal tract (iris, ciliary body, and choroid), and the internal neural layer (retina). At MRI, the outer layer appears hypointense on T1-weighted images and T2-weighted images, while the uveal tract and retina appear hyperintense on T1-weighted images and hypointense on T2-weighted images relative to the vitreous humor. The lens divides the globe into anterior and posterior segments.

Anterior Segment

Uveitis is defined as inflammation of the uveal tract. Anterior uveitis involves the anterior chamber and is often idiopathic or caused by noninfectious inflammatory diseases, such as ankylosing spondylitis and ulcerative colitis. Posterior uveitis involves the choroid and is typically associated with infectious diseases, such as toxoplasmosis (69). MRI features include thickening and enhancement of the uveal tract, subretinal effusions, and abnormal humor signal intensity (70).

Endophthalmitis is a globe infection affecting the vitreous or aqueous humor. Most cases arise either from direct organism inoculation due to trauma or ocular surgery or from hematogenous spread, often associated with immunodeficiency or intravenous drug use. Acute bacterial endophthalmitis is a vision-threatening emergency often requiring intravitreal antibiotic injection and possibly vitrectomy. Imaging findings include periocular inflammation, uveoscleral layer thickening and enhancement, and increased aqueous humor signal intensity on fluid-attenuated inversion-recovery MR images. Diffusion-weighted imaging facilitates diagnosis and treatment evaluation by revealing restricted diffusion in purulent exudates (Fig 22) (47, 70–72).

Lens

The lens is located in the hyaloid fossa and anchored to the ciliary bodies by zonular fibers. Ectopia lentis may occur following trauma or spontaneously, associated with Marfan syndrome and homocystinuria (47,73). A complete tear of the zonular fibers manifests as abnormal lens positioning, often settling in the posterior dependent portion of the globe. Anterior displacement is less common, as the iris restricts anterior lens movement. Partial tears lead to lens subluxation, resulting in angular displacement relative to its zonular attachments.

Posterior Segment

Retinoblastoma is the most common intraocular malignancy in children. Nearly all tumors develop following biallelic

Figure 23. Retinoblastoma in a 3-year-old girl who presented with left proptosis and vision loss. **(A)** Axial three-dimensional constructive interface in steady state MR image shows an irregular posterior wall lesion in the left globe exhibiting hypointense signal (white arrow) contiguous with optic nerve enlargement, suggestive of postlaminar invasion (arrowhead). Vitreous seeds are visible as discontinuous T2 hypointense foci (black arrow). **(B)** Axial diffusion-weighted MR image shows restricted diffusion in the tumor (white arrow) and the optic nerve (black arrow), supporting the diagnosis of malignancy. **(C)** Axial susceptibility-weighted image shows marked hypointense foci (arrow) corresponding to areas of calcification.

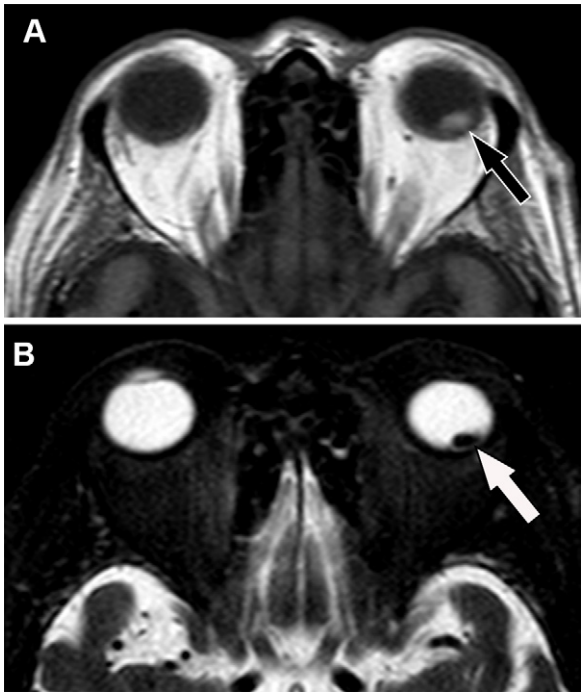

Figure 24. Uveal melanoma in a 57-year-old man who presented with left blurred vision. **(A)** Axial T1-weighted MR image shows a hyperintense well-defined nodule on the posterior wall of the left globe (arrow). **(B)** Axial T2-weighted MR image shows that the tumor displays a hypointense signal in relation to the vitreous humor (arrow). The signal characteristics of the tumor are indicative of pigmented uveal melanoma.

inactivation of the *RB1* tumor suppressor gene in precursor cells of the retinal neuroepithelium. Heritable retinoblastoma is characterized by *RB1* mutations in germline cells and is associated with earlier diagnosis, bilateral involvement, and multifocal disease. The median age at diagnosis for heritable retinoblastoma is 15 months, while for nonheritable disease it is 24 months (14,74).

Typical manifesting features are leukocoria, strabismus, and vision loss. Cross-sectional imaging is used to confirm the diagnosis and assess tumor extent. At MRI, retinoblastoma manifests as an irregular lesion, typically hypointense at T2-weighted imaging and slightly hyperintense at T1-weighted imaging compared with normal vitreous. Intralesional calcification is a key diagnostic feature and appears as a signal void on susceptibility-weighted sequences (Fig 23) (14,74,75).

Uveal melanoma is the most common primary intraocular malignancy in adults. Choroidal uveal melanoma is the most frequent subtype (90% of cases) and is associated with an aggressive course, often leading to hematogenous metastases (76). At MRI, uveal melanoma typically manifests as a well-defined tumor that is hyperintense at T1-weighted imaging and hypointense at T2-weighted imaging compared with normal vitreous. This characteristic imaging appearance is attributed to the paramagnetic effect of melanin, resulting in T1 and T2 shortening (Fig 24). Poorly pigmented tumors (20% of cases) may exhibit intermediate signal intensity on both T1-weighted and T2-weighted images (76). Strong pigmentation is associated with a less favorable prognosis. Expanding choroidal tumors may breach the Bruch membrane of the retina and extend into the subretinal space, assuming a mushroom shape. Further growth may also result in retinal detachment (10,76).

Retinal detachment occurs due to fluid accumulation in a potential space between the retinal pigmented epithelium and the inner sensory layer. Imaging shows a characteristic V shape due to firm attachments at the ora serrata and the optic disc (Fig 25). Conversely, choroidal detachment is attributed to fluid accumulation between the choroid and sclera. Imaging reveals a biconvex or lentiform fluid collection

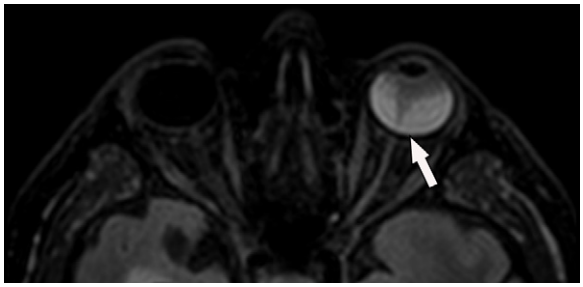

Figure 25. Retinal detachment in an 82-year-old man who presented with left vision loss. Axial fluid-attenuated inversion recovery–weighted MR image shows subretinal hemorrhage in the left globe (arrow). This is characterized by a hyperintense fluid collection relative to the normal vitreous humor, with a characteristic V-shaped appearance, anteriorly confined by the ora serrata and posteriorly limited by the optic disc.

extending anteriorly beyond the ora serrata and posteriorly confined by the insertion of the vortex veins (Fig 26) (47,77).

Conclusion

Interpreting studies using an anatomic approach can guide clinicians toward the most common pathologic conditions affecting each compartment of the orbit and provide a concise differential diagnosis. The Table summarizes the key imaging features and clinical insights. Since some pathologic conditions can involve multiple compartments and characteristic lesions may appear in atypical locations, the anatomic site should be considered along with other clinical and epidemiologic features and imaging findings to determine the most relevant diagnosis.

Author affiliations.—From the Department of Radiology, Head and Neck Section, Irmandade da Santa Casa de Misericórdia de São Paulo, R. Dr. Cesário Mota Júnior 112, Vila Buarque, São Paulo, SP 01221-010, Brazil (G.G.N., H.J.d.O.C., H.R.d.O., T.L.P.D.S., F.B.A.); Department of Radiology, Head and Neck Section, Grupo Fleury, São Paulo, SP, Brazil (T.L.P.D.S., H.B.Z., F.B.A.); Department of Radiology, Head and Neck Section, Hospital do Coração: São Paulo, São Paulo, Brazil (H.B.Z.); and Department of Radiology, Head and Neck Section, Instituto do Câncer do Estado de São Paulo, São Paulo, Brazil (H.B.Z.). Presented as an education exhibit at the 2023 RSNA Annual Meeting. Received January 29, 2024; revision requested April 15 and received May 27; accepted July 3. **Address correspondence to** G.G.N. (email: *guigotti@hotmail.com*).

Acknowledgments.—The authors express their gratitude for the invaluable assistance provided by Sílvia Marçal Benício de Mello, MD, Bruno Baldissara Moreira, Leonardo Furtado Freitas, MD, and Leandro Tavares Lucato, MD, PhD, in preparing the manuscript.

Disclosures of conflicts of interest.—All authors, the editor, and the reviewers have disclosed no relevant relationships.

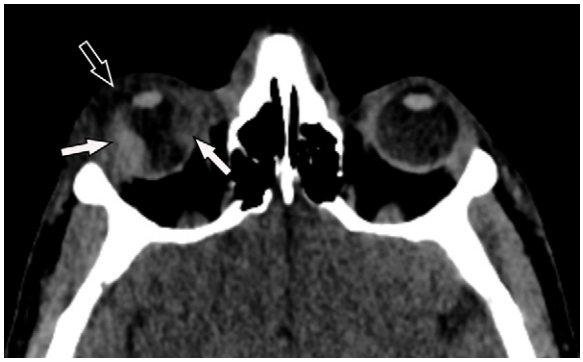

Figure 26. Choroidal detachment in a 45-year-old man who presented with right vision loss after trauma. Axial nonenhanced CT image shows biconvex hyperattenuation involving the right globe (white arrows), with relative sparing of the posterior aspect due to the insertion of the vortex veins. This morphology resembles that of a tennis ball. Periorbital edema is noted due to contusional trauma (black arrow).

References

1. Abel A, McClelland C, Lee MS. Critical review: Typical and atypical optic neuritis. Surv Ophthalmol 2019;64(6):770–779.
2. Ducloyer JB, Marignier R, Wiertlewski S, Lebranchu P. Optic neuritis classification in 2021. Eur J Ophthalmol 20211120672121102805O.
3. Petroulia VD, Brügger D, Hoepner R, et al. MRI signs helpful in the differentiation of patients with anterior ischaemic optic neuropathy and optic neuritis. Br J Ophthalmol 2023;107(1):121–126.
4. Dutra BG, da Rocha AJ, Nunes RH, Maia ACM. Neuromyelitis Optica Spectrum Disorders: Spectrum of MR Imaging Findings and Their Differential Diagnosis. RadioGraphics 2018;38(1):169–193 [Published correction appears in RadioGraphics 2018;38(2):662.]
5. Chen JJ, Flanagan EP, Jitprapaikulsan J, et al. Myelin Oligodendrocyte Glycoprotein Antibody-Positive Optic Neuritis: Clinical Characteristics, Radiologic Clues, and Outcome. Am J Ophthalmol 2018;195:8–15.
6. Remond P, Attyé A, Lecler A, et al. The Central Bright Spot Sign: A Potential New MR Imaging Sign for the Early Diagnosis of Anterior Ischemic Optic Neuropathy due to Giant Cell Arteritis. AJNR Am J Neuroradiol 2017;38(7):1411–1415.
7. Mournet S, Sené T, Charbonneau F, et al. Early diffusion-weighted MRI at 3 Tesla detects ischemic changes of the optic nerve in anterior ischemic optic neuropathy. Eur Radiol 2022;32(5):3588–3596.
8. Quddus A, Lawlor M, Siddiqui A, Holmes P, Plant GT. Using Diffusion-Weighted Magnetic Resonance Imaging to Confirm a Diagnosis of Posterior Ischaemic Optic Neuropathy: Two Case Reports and Literature Review. Neuroophthalmology 2015;39(4):161–165.
9. Czyzyk E, Jóźwiak S, Roszkowski M, Schwartz RA. Optic pathway gliomas in children with and without neurofibromatosis 1. J Child Neurol 2003;18(7):471–478.
10. Tailor TD, Gupta D, Dalley RW, Keene CD, Anzai Y. Orbital neoplasms in adults: clinical, radiologic, and pathologic review. RadioGraphics 2013;33(6):1739–1758.
11. Purohit BS, Vargas MI, Ailianou A, et al. Orbital tumours and tumour-like lesions: exploring the armamentarium of multiparametric imaging. Insights Imaging 2016;7(1):43–68.
12. Wang MX, Dillman JR, Guccione J, et al. Neurofibromatosis from head to toe: what the radiologist needs to know. RadioGraphics 2022;42(4):1123–1144.
13. Kornreich L, Blaser S, Schwarz M, et al. Optic pathway glioma: correlation of imaging findings with the presence of neurofibromatosis. AJNR Am J Neuroradiol 2001;22(10):1963–1969.
14. Joseph AK, Guerin JB, Eckel LJ, et al. Imaging findings of pediatric orbital masses and tumor mimics. RadioGraphics 2022;42(3):880–897.
15. Solli E, Turbin RE. Primary and Secondary Optic Nerve Sheath Meningioma. J Neurol Surg B Skull Base 2021;82(1):27–71.
16. Gupta S, Sethi P, Duvesh R, Sethi HS, Naik M, Rai HK. Optic perineuritis. BMJ Open Ophthalmol 2021;6(1):e000745.
17. ISSVA Classification of Vascular Anomalies. International Society for the Study of Vascular Anomalies. https://www.issva.org/classification. Published 2018. Accessed May 5, 2024.
18. Ansari SA, Mafee MF. Orbital cavernous hemangioma: role of imaging. Neuroimaging Clin N Am 2005;15(1):137–158.
19. Elbaze S, Duron L, Mambour N, et al. A signature of structural MRI features at 3 Tesla allows an accurate characterization of orbital cavernous venous malformation. Eur Radiol 2023;33(3):2149–2159.
20. Xian J, Zhang Z, Wang Z, et al. Evaluation of MR imaging findings differentiating cavernous haemangiomas from schwannomas in the orbit. Eur Radiol 2010;20(9):2221–2228.
21. Smoker WR, Gentry LR, Yee NK, Reede DL, Nerad JA. Vascular lesions of the orbit: more than meets the eye. RadioGraphics 2008;28(1):185–204; quiz 325.
22. Rootman J, Heran MK, Graeb DA. Vascular malformations of the orbit: classification and the role of imaging in diagnosis and treatment strategies*. Ophthal Plast Reconstr Surg 2014;30(2):91–104.

Imaging and Clinical Features of Orbital Pathologic Conditions

Pathologic Conditions	Characteristic Features	Differential Diagnosis
	ONSC	
Optic nerve gliomas (sporadic)	Masslike optic nerve enlargement with cystic components	Optic nerve sheath meningioma: enlargement of the ONSC due to peripheral tumor and "tram-track" sign
Optic nerve gliomas (NF1)	Optic nerve enlargement with increased tortuosity and frequently minimal enhancement; dural ectasia	
Optic nerve sheath meningioma	Optic nerve sheath thickening exhibiting homogeneous enhancement; intralesional calcifications; related to an NF2 diagnosis	Optic nerve pathway glioma: tumor indistinguishable from the nerve; related to an NF1 diagnosis
	Intraconal compartment	
CVM	Well-defined lesion with hyperintense signal on T2-weighted images and progressive enhancement with dynamic contrast sequences; more frequent in middle-aged women	Schwannoma: heterogeneous T2 signal intensity and immediate enhancement, frequently heterogeneous
Venous malformation (orbital varix)	Fusiform or teardrop-shaped lesion with hyperintense signal on T2-weighted images and avid immediate enhancement; distensible during Valsalva maneuver	CVM: nondistensible during Valsalva maneuver
LM	Transpatial lesions with hyperintense signal on T2-weighted images, cysts, and fluid-fluid levels with hemorrhagic components; poor contrast enhancement; more frequent in early childhood	Other vascular malformations: substantial contrast enhancement
Metastasis	Variable from well-defined and focal to ill-defined and invasive lesions; bone erosion; prior history of cancer	Variable depending on affected structure
	Conal compartment	
TED	Bilateral and symmetric EOM enlargement sparing tendinous insertions I'M SLOw involvement: IRM > MRM > SRM > LRM	IOI: unilateral; myotendinous junction involvement
Idiopathic orbital inflammation	Unilateral EOM enlargement with tubular morphology; local inflammatory changes; dacryoadenitis; optic perineuritis	IgG4-ROD: bilateral involvement; myotendinous junction sparing
IgG4-related disease	Bilateral EOM enlargement sparing tendinous insertions; local inflammatory changes; predominant LRM involvement; cranial nerve enlargement; dacryoadenitis	TED: late involvement of LRM; lacks other inflammatory findings
Conal lymphoma	Unilateral fusiform EOM enlargement exhibiting increased homogeneous enhancement; restricted diffusion with very low ADC	TED: follows typical involvement (I'M SLOw); lack of restricted diffusion
	Extraconal compartment	
IH	Well-defined lesion, exhibiting hyperintense signal on T2-weighted images and avid immediate enhancement; flow voids; characteristic in early childhood	Venous malformations: presence of phleboliths and lacks flow voids
Rhabdomyosarcoma	Aggressive lesion exhibiting hyperintense signal on T2-weighted images; contrast enhancement; bone erosion; restricted diffusion (ADC <1159 × 10^{-6} mm^2/sec); predominantly in young children	IH flow-voids; hyperintensity on ADC map
Schwannoma	Well-defined mixed solid-cystic lesion with heterogeneous enhancement; cone-shaped when involving orbital apex and dumbbell-shaped involving orbital fissures; related to an NF2 diagnosis	Neurofibromas: central hypointense area with surrounding hyperintense rim on T2-weighted images ("target sign"); related to an NF1 diagnosis
Lymphoma	Well-defined to invasive lesions with homogeneous enhancement; molds to surrounding structures; restricted diffusion with very low ADC (lower than 612 × 10^{-6} mm^2/sec)	IgG4-ROD and IOI: lack of restricted diffusion
	Lacrimal apparatus	
Pleomorphic adenoma	Well-defined lesion with hyperintense signal on T2-weighted images and heterogeneous enhancement; cystic degeneration; bone remodeling	Signs of malignant tumor: bone erosion; poorly defined margins; invasive lesion; perineural invasion
Malignant lacrimal tumor	Early lesions exhibit well-defined margins progressing to poorly defined and invasive lesions; bone erosion; restricted diffusion	
Dacryoadenitis	Diffuse gland enlargement and adjacent fat stranding; marked contrast enhancement	Lacrimal lymphoma: restricted diffusion, frequently with very low ADC; acute gland enlargement in the context of chronic enlargement
	Globe compartment	
Retinoblastoma	Posterior wall lesion exhibiting hypointense signal on T2-weighted images; intralesional calcification; restricted diffusion; affects young children; leukocoria	Coats disease: lack of calcification; atrophied optic nerve
Uveal melanoma	Most commonly a posterior wall lesion; pigmented tumors exhibit hyperintense signal on T1-weighted images; restricted diffusion	Uveal metastasis: bilateral lesions; lacks hyperintense signal intensity on T1-weighted images
Retinal detachment	V-shaped liquid fluid collections, limited anteriorly by the ora serrata and posteriorly by the optic disc	Choroidal detachment; anterior extension beyond the ora serrata
Choroidal detachment	Biconvex fluid collections; "tennis ball" morphology extending to the anterior portion of the globe and posteriorly confined by the vortex veins	Retinal detachment: limited anteriorly by the ora serrata

Note.—ADC = apparent diffusion coefficient, IOI = idiopathic orbital inflammation, IRM = inferior rectus muscle, LRM = lateral rectus muscle, MRM = medial rectus muscle, SRM = superior rectus muscle.

23. Mavrikakis I, Heran MK, White V, Rootman J. The role of thrombosis as a mechanism of exacerbation in venous and combined venous lymphatic vascular malformations of the orbit. Ophthalmology 2009;116(6):1216–1224.
24. Katz SE, Rootman J, Vangveeravong S, Graeb D. Combined venous lymphatic malformations of the orbit (so-called lymphangiomas). Association with noncontiguous intracranial vascular anomalies. Ophthalmology 1998;105(1):176–184.
25. Ahmad SM, Esmaeli B. Metastatic tumors of the orbit and ocular adnexa. Curr Opin Ophthalmol 2007;18(5):405–413.
26. Palmisciano P, Ferini G, Ogasawara C, et al. Orbital Metastases: A Systematic Review of Clinical Characteristics, Management Strategies, and Treatment Outcomes. Cancers (Basel) 2021;14(1):94.
27. Glisson CC. Approach to Diplopia. Continuum (Minneap Minn) 2019;25(5):1362–1375 [Published correction appears in Continuum (Minneap Minn) 2020;26(1):240].
28. Bartalena L, Piantanida E, Gallo D, Lai A, Tanda ML. Epidemiology, Natural History, Risk Factors, and Prevention of Graves' Orbitopathy. Front Endocrinol (Lausanne) 2020;11:615993.
29. Debnam JM, Koka K, Esmaeli B. Extrathyroidal Manifestations of Thyroid Disease: Graves Eye Disease. Neuroimaging Clin N Am 2021;31(3):367–378.
30. Burch HB, Perros P, Bednarczuk T, et al. Management of thyroid eye disease: a Consensus Statement by the American Thyroid Association and the European Thyroid Association. Eur Thyroid J 2022;11(6):e220189.
31. Lakerveld M, van der Gijp A. Orbital Muscle Enlargement: What if It's Not Graves' Disease? Curr Radiol Rep 2022;10(2):9–19.
32. Tortora F, Prudente M, Cirillo M, et al. Diagnostic accuracy of short-time inversion recovery sequence in Graves' Ophthalmopathy before and after prednisone treatment. Neuroradiology 2014;56(5):353–361.
33. Rana K, Garg D, Patel S, Selva D. Imaging of dysthyroid optic neuropathy. Eur J Ophthalmol 2023;0(0):11206721231199367.
34. Rutkowska-Hinc B, Maj E, Jabłońska A, Milczarek-Banach J, Bednarczuk T, Miśkiewicz P. Prevalence of Radiological Signs of Dysthyroid Optic Neuropathy in Magnetic Resonance Imaging in Patients with Active, Moderate-to-Severe, and Very Severe Graves Orbitopathy. Eur Thyroid J 2018;7(2):88–94.
35. McNab AA. Orbital Myositis: A Comprehensive Review and Reclassification. Ophthal Plast Reconstr Surg 2020;36(2):109–117.
36. Ben Artsi E, Mckelvie PA, McNab AA. Histopathologic Findings in Idiopathic Orbital Myositis. Ophthalmology 2021;128(4):609–616.
37. Mombaerts I, McNab AA. Idiopathic Orbital Myositis Revisited. Curr Rheumatol Rep 2022;24(1):20–26.
38. Yuen SJ, Rubin PA. Idiopathic orbital inflammation: distribution, clinical features, and treatment outcome. Arch Ophthalmol 2003;121(4):491–499.
39. Tiegs-Heiden CA, Eckel LJ, Hunt CH, et al. Immunoglobulin G4-related disease of the orbit: imaging features in 27 patients. AJNR Am J Neuroradiol 2014;35(7):1393–1397.
40. Sogabe Y, Ohshima K, Azumi A, et al. Location and frequency of lesions in patients with IgG4-related ophthalmic diseases. Graefes Arch Clin Exp Ophthalmol 2014;252(3):531–538.
41. Kim N, Yang HK, Kim JH, Hwang JM. IgG4-related ophthalmic disease involving extraocular muscles: case series. BMC Ophthalmol 2018;18(1):162.
42. Surov A, Behrmann C, Holzhausen HJ, Kösling S. Lymphomas and metastases of the extra-ocular musculature. Neuroradiology 2011;53(11):909–916.
43. Leung V, Wei M, Roberts TV. Metastasis to the extraocular muscles: a case report, literature review and pooled data analysis. Clin Exp Ophthalmol 2018;46(6):687–694.
44. Watkins LM, Carter KD, Nerad JA. Ocular adnexal lymphoma of the extraocular muscles: case series from the University of Iowa and review of the literature. Ophthal Plast Reconstr Surg 2011;27(6):471–476.
45. Savino G, Midena G, Tartaglione T, Milonia L, Caputo CG, Grimaldi G. Clinical-Radiological Patterns and Histopathological Outcomes in Non-Thyroid Extraocular Muscle Enlargement: Retrospective Case Series and Current Concepts. Ophthal Plast Reconstr Surg 2020;36(3):284–291.
46. Priego G, Majos C, Climent F, Muntane A. Orbital lymphoma: imaging features and differential diagnosis. Insights Imaging 2012;3(4):337–344.
47. Nguyen VD, Singh AK, Altmeyer WB, Tantiwongkosi B. Demystifying Orbital Emergencies: A Pictorial Review. RadioGraphics 2017;37(3):947–962.
48. Nagaraj UD, Koch BL. Imaging of orbital infectious and inflammatory disease in children. Pediatr Radiol 2021;51(7):1149–1161.
49. Santos JC, Pinto S, Ferreira S, Maia C, Alves S, da Silva V. Pediatric preseptal and orbital cellulitis: A 10-year experience. Int J Pediatr Otorhinolaryngol 2019;120:82–88.
50. Tsirouki T, Dastiridou AI, Ibánez Flores N, et al. Orbital cellulitis. Surv Ophthalmol 2018;63(4):534–553.
51. Haik BG, Karcioglu ZA, Gordon RA, Pechous BP. Capillary hemangioma (infantile periocular hemangioma). Surv Ophthalmol 1994;38(5):399–426.
52. Haik BG, Jakobiec FA, Ellsworth RM, Jones IS. Capillary hemangioma of the lids and orbit: an analysis of the clinical features and therapeutic results in 101 cases. Ophthalmology 1979;86(5):760–792.
53. Chang LC, Haggstrom AN, Drolet BA, et al; Hemangioma Investigator Group. Growth characteristics of infantile hemangiomas: implications for management. Pediatrics 2008;122(2):360–367.
54. Conneely MF, Mafee MF. Orbital rhabdomyosarcoma and simulating lesions. Neuroimaging Clin N Am 2005;15(1):121–136.
55. Jawad N, McHugh K. The clinical and radiologic features of paediatric rhabdomyosarcoma. Pediatr Radiol 2019;49(11):1516–1523.
56. Sepahdari AR, Aakalu VK, Setabutr P, Shiehmorteza M, Naheedy JH, Mafee MF. Indeterminate orbital masses: restricted diffusion at MR imaging with echo-planar diffusion-weighted imaging predicts malignancy. Radiology 2010;256(2):554–564.
57. Kralik SF, Haider KM, Lobo RR, Supakul N, Calloni SF, Soares BP. Orbital infantile hemangioma and rhabdomyosarcoma in children: differentiation using diffusion-weighted magnetic resonance imaging. J AAPOS 2018;22(1):27–31.
58. Kapur R, Mafee MF, Lamba R, Edward DP. Orbital schwannoma and neurofibroma: role of imaging. Neuroimaging Clin N Am 2005;15(1):159–174.
59. Sweeney AR, Gupta D, Keene CD, et al. Orbital peripheral nerve sheath tumors. Surv Ophthalmol 2017;62(1):43–57.
60. Wang Y, Xiao LH. Orbital schwannomas: findings from magnetic resonance imaging in 62 cases. Eye (Lond) 2008;22(8):1034–1039.
61. Pointdujour-Lim R, Lally SE, Shields JA, Eagle RC Jr, Shields CL. Orbital Schwannoma: Radiographic and Histopathologic Correlation in 15 Cases. Ophthal Plast Reconstr Surg 2018;34(2):162–167.
62. Akansel G, Hendrix L, Erickson BA, et al. MRI patterns in orbital malignant lymphoma and atypical lymphocytic infiltrates. Eur J Radiol 2005;53(2):175–181.
63. Olsen TG, Heegaard S. Orbital lymphoma. Surv Ophthalmol 2019;64(1):45–66.
64. Haradome K, Haradome H, Usui Y, et al. Orbital lymphoproliferative disorders (OLPDs): value of MR imaging for differentiating orbital lymphoma from benign OPLDs. AJNR Am J Neuroradiol 2014;35(10):1976–1982.
65. Gao Y, Moonis G, Cunnane ME, Eisenberg RL. Lacrimal gland masses. AJR Am J Roentgenol 2013;201(3):W371–W381.
66. Vora Z, Hemachandran N, Sharma S. Imaging of Lacrimal Gland Pathologies: A Radiological Pattern-Based Approach. Curr Probl Diagn Radiol 2021;50(5):738–748.
67. Singh S, Selva D. Non-infectious Dacryoadenitis. Surv Ophthalmol 2022;67(2):353–368.
68. Tonami H, Matoba M, Yokota H, Higashi K, Yamamoto I, Sugai S. CT and MR findings of bilateral lacrimal gland enlargement in Sjögren syndrome. Clin Imaging 2002;26(6):392–396.
69. Miserocchi E, Fogliato G, Modorati G, Bandello F. Review on the worldwide epidemiology of uveitis. Eur J Ophthalmol 2013;23(5):705–717.
70. Li CQ, Cho AA, Edward NJ, Edward DP, Fajardo RG, Mafee MF. Magnetic resonance imaging of uveitis. Neuroradiology 2015;57(8):825–832.
71. Radhakrishnan R, Cornelius R, Cunnane MB, Golnik K, Morales H. MR imaging findings of endophthalmitis. Neuroradiol J 2016;29(2):122–129.
72. Rumboldt Z, Moses C, Wieczerzynski U, Saini R. Diffusion-weighted imaging, apparent diffusion coefficients, and fluid-attenuated inversion recovery MR imaging in endophthalmitis. AJNR Am J Neuroradiol 2005;26(7):1869–1872.
73. Netland KE, Martinez J, LaCour OJ 3rd, Netland PA. Traumatic anterior lens dislocation: a case report. J Emerg Med 1999;17(4):637–639.
74. Pai V, Lin XY, Marcus M, et al. Diagnostic imaging for retinoblastoma cancer staging: guide for providing essential insights for ophthalmologists and oncologists. RadioGraphics 2024;44(4)e230125 [Published correction appears in RadioGraphics 2024;44(4):e249003.]
75. Silvera VM, Guerin JB, Brinjikji W, Dalvin LA. Retinoblastoma: What the Neuroradiologist Needs to Know. AJNR Am J Neuroradiol 2021;42(4):618–626.
76. Foti PV, Travali M, Farina R, et al. Diagnostic methods and therapeutic options of uveal melanoma with emphasis on MR imaging-Part I: MR imaging with pathologic correlation and technical considerations. Insights Imaging 2021;12(1):66.
77. Mafee MF, Karimi A, Shah JD, Rapoport M, Ansari SA. Anatomy and pathology of the eye: role of MR imaging and CT. Magn Reson Imaging Clin N Am 2006;14(2):249–270.